PLOS | ONE

RESEARCH ARTICLE

Respiration-Averaged CT for Attenuation Correction of PET Images – Impact on PET Texture Features in Non-Small Cell Lung Cancer Patients

Nai-Ming Cheng[1,2], Yu-Hua Dean Fang[3], Din-Li Tsan[4], Ching-Han Hsu[2☯], Tzu-Chen Yen[1☯*]

1 Departments of Nuclear Medicine, Chang Gung Memorial Hospita, Linkou, Chang Gung University College of Medicine, Taoyuan City 33305, Taiwan, **2** Department of Biomedical Engineering and Environmental Sciences, National Tsing Hua University, Hsinchu City, 30071, Taiwan, **3** Department of Biomedical Engineering, National Cheng Kung University, Tainan City, 70101, Taiwan, **4** Department of Radiation Oncology, Chang Gung Memorial Hospital, Chang Gung University College of Medicine, Taoyuan City 33305, Taiwan

☯ These authors contributed equally to this work.
* yentc1110@gmail.com

Citation: Cheng N-M, Fang Y-HD, Tsan D-L, Hsu C-H, Yen T-C (2016) Respiration-Averaged CT for Attenuation Correction of PET Images – Impact on PET Texture Features in Non-Small Cell Lung Cancer Patients. PLoS ONE 11(3): e0150509. doi:10.1371/journal.pone.0150509

Editor: Quan Sing Ng, National Cancer Centre Singapore, SINGAPORE

Received: August 21, 2015

Accepted: February 14, 2016

Published: March 1, 2016

Data Availability Statement: All relevant data are within the paper and its Supporting Information files.

Funding: The authors received no specific funding for this work.

Competing Interests: The authors have declared that no competing interests exist.

Abstract

Purpose

We compared attenuation correction of PET images with helical CT (PET/HCT) and respiration-averaged CT (PET/ACT) in patients with non-small-cell lung cancer (NSCLC) with the goal of investigating the impact of respiration-averaged CT on ^{18}F FDG PET texture parameters.

Materials and Methods

A total of 56 patients were enrolled. Tumors were segmented on pretreatment PET images using the adaptive threshold. Twelve different texture parameters were computed: standard uptake value (SUV) entropy, uniformity, entropy, dissimilarity, homogeneity, coarseness, busyness, contrast, complexity, grey-level nonuniformity, zone-size nonuniformity, and high grey-level large zone emphasis. Comparisons of PET/HCT and PET/ACT were performed using Wilcoxon signed-rank tests, intraclass correlation coefficients, and Bland-Altman analysis. Receiver operating characteristic (ROC) curves as well as univariate and multivariate Cox regression analyses were used to identify the parameters significantly associated with disease-specific survival (DSS). A fixed threshold at 45% of the maximum SUV (T45) was used for validation.

Results

SUV maximum and total lesion glycolysis (TLG) were significantly higher in PET/ACT. However, texture parameters obtained with PET/ACT and PET/HCT showed a high degree of agreement. The lowest levels of variation between the two modalities were observed for SUV entropy (9.7%) and entropy (9.8%). SUV entropy, entropy, and coarseness from both

PET/ACT and PET/HCT were significantly associated with DSS. Validation analyses using T45 confirmed the usefulness of SUV entropy and entropy in both PET/HCT and PET/ACT for the prediction of DSS, but only coarseness from PET/ACT achieved the statistical significance threshold.

Conclusions

Our results indicate that 1) texture parameters from PET/ACT are clinically useful in the prediction of survival in NSCLC patients and 2) SUV entropy and entropy are robust to attenuation correction methods.

Introduction

Despite significant advances in targeted therapy [1], the prognosis of patients with non-small cell lung cancer (NSCLC) remains dismal. ^{18}F-FDG PET imaging plays an essential role in the diagnosis and staging of NSCLC. Recent years have witnessed an increased use of FDG PET imaging for clinical decision making [2]. Accordingly, maximum standardized uptake values (SUV_{max}) [3, 4] and total lesion glycolysis (TLG) [5, 6] have been shown to be clinically useful for predicting treatment response and clinical outcomes of NSCLC patients. Tumor heterogeneity has been generally related to poor prognosis and treatment resistance [7]. Growing evidence indicates that FDG PET texture features reflecting tumor heterogeneity may predict therapeutic response and survival in NSCLC [8–11] and numerous other malignancies [12–20]. The mining of a large number of quantitative image features has been referred to "radiomics" and holds promise as a method for identifying specific prognostic signatures [10, 21–26]. In this scenario, accurate and reproducible measurements of texture features are essential for clinical use. Unfortunately, respiratory motion during PET/CT results in degradation of image quality and hampers the correct quantification of imaging parameters [27–29]. Such deterioration is caused by the discrepancy of chest position between helical CT (HCT) and PET images [30, 31]. Rather than a snapshot of the respiration cycle (as in HCT images), PET scans are the results of the average of respiratory cycles. Notably, the temporal difference between PET and CT ultimately introduces misalignment artifacts in PET images. To address this issue, attenuation correction of PET images with respiration averaged CT (ACT) has been utilized. Rather than providing a motionless CT image, ACT simulates the PET acquisition process by averaging the signal during a respiratory cycle from multiple low-dose cine CT images. Previous studies have shown that ACT correction can improve the quality of PET images by reducing misalignments and optimizing the quantification of SUV [31–34]. Nevertheless, the utility of ACT for correcting PET texture features has not been thoroughly investigated. In addition, data on the potential prognostic impact of different PET texture features in NSCLC patients remain scarce. Because of the increasing use of ^{18}F-FDG PET/CT in clinical trials, an analysis of the variability related to attenuation correction is worthy of investigation. We therefore designed the current study to compare attenuation correction of PET images with HCT and ACT in NSCLC with the goal of investigating the impact of respiration-averaged CT on FDG PET texture parameters.

Materials and Methods

Patients

The Institutional Review Board of the Chang Gung Memorial Hospital at Linkou approved the study protocol (102-3810B). Written informed consent was obtained from all patients before

ACT. The study population consisted of patients with pathologically-proven NSCLC who were scheduled to undergo definitive treatment with curative intent. All of the study participants underwent ^{18}F-FDG PET for disease staging. The treatment approach was as follows: 1) radical surgery for stage IA patients, 2) radical surgery plus adjuvant chemotherapy for stage IB and IIA patients, 3) neoadjuvant therapy (chemotherapy, radiotherapy, or concurrent chemoradiotherpy [CCRT]) and operation for stage IIB and IIIA patients, and 4) chemotherapy, radiotherapy, or CCRT and operation (in presence of resectable disease) for stage IIIB patients. Patients with M1 disease were excluded. Patients were staged according to the 2010 (7th edition) American Joint Committee on Cancer (AJCC) staging system. We retrospectively reviewed the clinical charts to extract the general characteristics and the clinical outcomes of the participants. Disease-specific survival (DSS) – defined as the time from diagnosis to NSCLC-related death – served as the main outcome measure.

PET/CT imaging protocol

Patients were asked to fast 6 h before examination. According to our institutional policy, patients with blood glucose levels greater than 200 mg/dL had their scan rescheduled. All participants were imaged using the same PET/CT scanner (Discovery ST16, GE Healthcare). Scans were obtained 50 min after intravenous FDG administration. The injected dose of FDG was calculated according to body weight and ranged between 370 and 555 MBq. HCT data were acquired with the following settings: 120 kV, automatic mA (range: 10–300 mA), pitch 1.75:1, collimation 16×3.75 mm, and rotation cycle 0.5 s. Whole-body PET emission scans were performed in the 2D mode and acquired from the skull to the mid-thigh. Following HCT and PET acquisition, a low-dose cine CT was performed using the following settings: 120 kV, automatic mA (range: 10–25 mA according to the patient's body weight), rotation cycle 0.5 s, collimation 8×2.5 mm, and cine duration 5.9 s. The goal was to include lung fields bilaterally from the pulmonary apex to the dome of the liver [32, 35–37]. Ten phases of cine CT images were averaged to obtain ACT. No intravenous contrast enhancement was used, and imaging was performed in the free-breathing state. No pre- or in-scan breathing coach for respiratory control was used. Attenuation correction of PET images was performed with both HCT and ACT using the same PET data [30, 32, 35]. PET emission data were reconstructed with attenuation correction using both HCT and ACT attenuation maps. Transaxial emission images were reconstructed using ordered subsets expectation maximization (OSEM) with 4 iterations and 10 subsets. PET images were reconstructed on a 128 × 128 image matrix with a voxel size of $4.46 \times 5.46 \times 3.27$ mm^3 for both PET/HCT and PET/ACT. An additional dose of 2.5 mSv (5 mGy) was used for patients with a body weight > 70 kg [38].

PET/CT image data analysis

The PMOD 3.3 software package (PMOD Technologies Ltd, Zurich, Switzerland) was used for tumor segmentation. We applied two methods for tumor segmentation, i.e. (1) the adaptive threshold approach in the exploratory analysis and (2) 45% of SUV_{max} (T45) for validation purposes. The adaptive threshold was determined by using a mean intensity of voxel contoured by 70% of the tumor SUVmax ($I_{mean\ 70\%}$) plus the background mean SUV [39]. The aortic arch was used for background measurement and none of the study participants had aortic arch invasion. Two authors (N.M.C. and T.C.Y.) contoured the aortic arch using 1 cm^3 cubic volumes of interest (VOI) and results were averaged. Care was taken to exclude calcified regions in the aortic arch. Finally, the adaptive threshold was calculated according to the following formula: $0.15 \times (I_{mean\ 70\%})$ + background. The T45 approach has been previously utilized for delineation of NSCLC tumors [8]. SUV_{max}, mean SUV, and texture features were determined

using the tumor VOI. TLG was calculated as follows: TLG = mean SUV × metabolic tumor volume (MTV) [40]. We did not analyze nodal lesions because of their small size.

Histogram analysis, normalized grey-level co-occurrence matrix (NGLCM) [41, 42], neighborhood grey-tone difference matrix (NGTDM)[43], and grey level size zone matrix (GLSZM) [44] were applied for calculation of PET texture features. Because numerous texture features have been reported [12, 45, 46], we specifically focused on those utilized for predicting survival in patients with malignancies. Several texture parameters, including entropy, uniformity, homogeneity and dissimilarity from NGLCM [11, 14, 47, 48], grey-level nonuniformity (GLNU), zone-size nonuniformity (ZSNU), high grey-level large zone emphasis (HGLZE) from GLSZM [14, 19], and NGTDM based coarseness, busyness, contrast and complexity [8] have been used for survival prediction in patients with NSCLC, esophageal cancer, and head and neck malignancies. In addition, we evaluated SUV entropy based on histogram analysis because of its robustness due to different reconstruction settings [45, 49]. A total of 12 different texture features were examined. The intensity values of the recorded VOIs were initially resampled into 64 bins to normalize images and reduce noise for the calculation of texture features [13]. The computations for texture features were performed using the Chang-Gung Image Texture Analysis toolbox (CGITA) implemented under MATLAB 2012a (Mathworks Inc., Natick, MA, USA). The details on mathematical models for texture matrices and the calculation process have been previously described in detail [14, 50].

Statistical analysis

Because most texture features showed a skewed distribution, the non-parametric Wilcoxon signed-rank test was used for paired comparisons of PET/HCT and PET/ACT parameters. The reciprocal associations of texture features in PET/HCT and PET/ACT were examined using intraclass correlation coefficients (ICC). Precision was defined by half of the width of the 95% confidence intervals (CIs) and used as an indicator of reliability. Bland-Altman analysis was used for comparing two measurements. The differences between the two parameters (i.e., PET/ACT values minus PET/HCT values) were plotted against their average (e.g. mean of PET/HCT and PET/ACT values) and reported as percentage. The lower and upper reproducibility limits (LRL and URL, respectively) were calculated as ± 1.96 standard deviations (SD). Variations were defined as the range between LRL and URL. In an exploratory analysis, the evaluation of texture parameters was based on a step-forward process. The median follow-up time in the entire study cohort was 26.2 months (range: 2.5–74.8 months), whereas it was 59.0 months (range: 40.4–74.8 months) in patients who survived. Because all of the enrolled cases were followed up of at least 3 years or until death, receiver operating characteristic (ROC) curves were initially used to identify the image features associated with 3-year DSS. All of the parameters with an area under curve different from 0.5 were selected for further analyses. The optimal cutoff values were identified by determining the point where the sum of sensitivity and specificity (Youden's index) was maximum. Dichotomizing patients according to the optimal cutoff values were used in subsequent univariate and multivariate Cox regression analyses. Because of the high collinearity among different texture features, we constructed multivariate Cox regression models to include only one texture parameter and the following covariates: age, cell type (adenocarcinoma *vs*. non-adenocarcinoma), AJCC stage (stage I, II *vs*. stage III), and radical surgery (yes *vs*. no). All calculations were performed with the PASW Statistics 18 software package (SPSS Inc., Chicago, IL, USA). After application of the Bonferroni correction, a P value < 0.017 (i.e., 0.05/3) was considered statistically significant.

Results

Patients

Between July, 2007 and June, 2009, a total of 56 consecutive patients (36 males, 20 females; median age: 68 years; age range: 34–84 years) were enrolled. The median follow-up time in the entire study cohort was 26.2 months (range: 2.5–74.8 months), whereas it was 59.0 months (range: 40.4–74.8 months) in patients who survived. The clinical characteristics of the study participants are shown in Table 1. The most common histological type was adenocarcinoma (n = 31, 55.4%), and the majority of patients were diagnosed at advanced stages (stage IIIA or IIIB, n = 36, 64.2%). Twenty-two (39.3%) tumors were located in the lower pulmonary lobes, whereas 34 (60.7%) were located in the upper or right middle lobes. A total of 29 patients (51.8%) received radical surgery. The median glucose level before FDG PET imaging was 93 mg/dL (range: 65–151 mg/dL). There were no significant interobserver differences in background activity for both PET/HCT (observer 1 *vs*. 2: 1.60 ± 0.30 vs. 1.62 ± 0.31, P = 0.325) and PET/ACT (1.65 ± 0.34 *vs*. 1.65 ± 0.32, P = 0.960). No differences were noted in the values of resulting adaptive thresholds (2.88 ± 0.80 *vs*. 2.91 ± 0.81, P = 0.318 and 2.96 ± 0.82 *vs*. 2.96 ± 0.83, P = 0.954 for PET/HCT and PET/ACT, respectively). Using the mean threshold for tumor delineation, the median MTV for PET/HCT and PET/ACT were 26.19 cm^3 and 26.58 cm^3, respectively (Wilcoxon signed-ranks test, $P = 0.426$).

Table 1. Clinicopathological characteristics of the study patients.

Characteristic	n (%)
Sex	
Male	36 (64.3)
Female	20 (35.7)
Age (years)	
Range	34–84
Median	68
Sites of tumors	
Lower lobe	22 (39.3)
Other lobes	34 (60.7)
TNM stage	
T1	5 (8.9)
T2	28 (50.0)
T3	3 (5.4)
T4	20 (35.7)
N0	20 (35.7)
N1	10 (17.9)
N2	19 (33.9)
N3	7 (12.5)
AJCC Stage	
IA	3 (5.4)
IB	11 (19.6)
IIA	2 (3.6)
IIB	4 (7.1)
IIIA	11 (19.6)
IIIB	25 (44.6)

doi:10.1371/journal.pone.0150509.t001

Table 2. Results of Wilcoxon signed-ranks tests for PET/HCT and PET/ACT parameters.

Variables	PET/HCT			PET/ACT			*P*
	Mean	SD	Range	Mean	SD	Range	
SUV_{max}	11.12	5.95	3.03–36.05	11.29	6.03	3.08–36.74	0.009
SUV mean	5.05	2.16	2.01–13.03	5.16	2.22	2.01–13.80	<0.001
TLG	273.5	378.5	2.7–1802.8	287.0	403.3	2.6–1846.7	<0.001
Texture parameters							
SUV entropy	3.71	0.26	2.66–4.02	3.72	0.26	2.74–4.01	0.516
Uniformity	0.003	0.004	0.001–0.02	0.003	0.003	0.001–0.02	0.853
Entropy	6.35	0.82	3.76–7.30	6.35	0.81	3.97–7.28	0.734
Dissimilarity	8.83	2.71	4.85–19.13	8.84	2.76	4.65–19.21	0.766
Homogeneity	0.19	0.04	0.12–0.27	0.19	0.04	0.12–0.28	0.969
Coarseness	0.030	0.022	0.002–0.09	0.030	0.02	0.002–0.09	0.780
Busyness	0.222	0.296	0.021–1.528	0.224	0.303	0.020–1.503	0.411
Contrast	0.081	0.335	0.0004–2.336	0.075	0.307	0.0004–2.136	0.382
Complexity	52.35	68.94	0.98–277.8	51.26	64.22	0.95–273.4	0.256
Grey-level nonuniformity	9.67	11.78	1.00–67.36	9.73	11.89	1.12–66.15	0.714
Zone-size nonuniformity	214.9	231.6	10.2–1231.3	214.1	232.8	15.1–1262.4	0.914
High grey-level large zone emphasis	2564	1461	1012–7223	2685	1652	891–10488	0.154

SUV, standardized uptake value; TLG: total lesion glycolysis.

doi:10.1371/journal.pone.0150509.t002

PET image analysis

The results of Wilcoxon sign-ranks tests revealed that PET/ACT yielded significant higher SUV_{max}, SUV mean, and TLG values. However, all of the texture parameters did not show significant differences (Table 2). Specifically, SUV_{max} of tumors located in the lower lung were significantly higher in PET/ACT, but similar values were noted for tumors arising in other sites (S1 Table). Despite differences in SUV_{max}, SUV mean, and TLG between PET/HCT and PET/ACT, ICC analysis revealed a high degree of correlation and good precision (ICC: 0.993, 0.994, and 0.993; precision: 0.35, 0.35, and 0.40% for SUV_{max}, SUV mean, and TLG, respectively). HGLZE showed the lowest levels of correlation and precision (0.919 and 4.35%, respectively). High correlation coefficients (ICC $>$ 0.95) were generally noted for other texture features (Table 3). The variations of SUV_{max} and SUV mean in Bland-Altman analysis were 25.4% and 18.1%, respectively. The lowest level of variation was evident for SUV entropy (9.7%) followed by entropy (9.8%), as revealed in Fig 1. Among NGTDM and GLSZM parameters, coarseness and GLNU had the lowest degree of variation (33.0% and 45.2%, respectively). The highest levels of variation were noted for contrast (104.9%) and HGLZM (80.6%), S1 Fig. Variation values greater than 50% were evident for uniformity (56.6%), busyness (52.9%), complexity (67.1%), ZSNU (74.4%), and HGLZE (80.6%). High degrees of correlation between texture parameters ($|\rho|$ = 0.614–0.993 for PET/HCT and $|\rho|$ = 0.567–0.993 for PET/ACT, all $P < 0.001$) were evident for both PET/ACT and PET/HCT.

Survival analysis

At the end of study, 36 patients died (35 of NSCLC and one of acute myocardial infarction). A total of 47 patients (83.9%) had disease progression during follow-up. Three methods (ROC curve analyses, univariate Cox regression analysis, multivariate Cox regression analysis) were

Table 3. Intraclass correlation coefficients and Bland-Altman analyses of PET parameters.

Variables	Intraclass Correlation Coefficient (ICC)			Bland-Altman analysis		
	ICC	95% CI	Precision (%)	Mean	Variation (%)	LRL[a]–URL[b] (%)
SUV_{max}	0.993	0.989–0.996	0.35	1.5	25.4	-11.2–14.2
SUV mean	0.994	0.990–0.997	0.35	2.3	18.1	-6.7–11.4
TLG	0.993	0.988–0.996	0.40	3.5	43.8	-18.4–25.4
Texture parameters						
SUV entropy	0.949	0.915–0.970	2.75	0.1	9.7	-4.7–5.0
Uniformity	0.956	0.926–0.974	2.40	0.2	56.6	-28.1–28.5
Entropy	0.987	0.978–0.992	0.70	0	9.8	-4.90–4.90
Dissimilarity	0.975	0.964–0.987	1.15	-0.1	22.7	-11.4–11.3
Homogeneity	0.977	0.962–0.987	1.25	-0.4	16.7	-8.7–8.0
Coarseness	0.982	0.970–0.990	1.00	-0.6	33.0	-17.1–15.9
Busyness	0.996	0.993–0.998	0.25	-0.6	52.9	-27.1–25.8
Contrast	0.983	0.971–0.990	0.95	-2.3	104.9	-54.8–50.1
Complexity	0.975	0.958–0.986	1.40	-1.0	67.1	-34.5–32.6
Grey-level nonuniformity	0.998	0.997–0.999	0.10	-1.5	45.2	-24.1–21.1
Zone-size nonuniformity	0.997	0.994–0.998	0.20	-1.2	74.4	-38.4–36.0
High grey-level large zone emphasis	0.919	0.865–0.952	4.35	4.5	80.6	-35.4–44.8

[a]LRL: lower reproducibility limit

[b]URL: upper reproducibility limit.

doi:10.1371/journal.pone.0150509.t003

used to investigate the prognostic role of texture parameters. The results of ROC curve analyses (S2 Table) revealed that SUV entropy, uniformity, entropy, coarseness, contrast, GLNU, and ZSNU from PET/HCT and PET/ACT were statistically significant. When patients were dichotomized according to the optimal cutoff values, we found a high consistency of texture parameters derived from PET/HCT and PET/ACT. Identifcal stratification results were obtained with regard to entropy and coarseness; 55 of 56 cases (98.2%) were based on the cut-off for GLNU; 54 (96.4%) for ZSNU; 53 (94.6%) for uniformity and 50 (89.3%) for SUV entropy. ICC, precision, and variation did not show significant associations with stratification consistency (Spearman's ρ = -0.211, 0.266 and -0.248, P = 0.559, 0.457 and 0.490, respectively). Subsequently analyses using univariate and multivariate Cox models confirmed the significant role of SUV entropy, entropy, and coarseness from both PET/HCT and PET/ACT in the prediction of DSS (Table 4). The complete results of univariate and multivariate Cox regression analyses are shown in S5 Table. Kaplan-Meier estimates of DSS for PET/HCT and PET/ACT parameters are shown in Fig 2.

Validation data

MTV and TLG delineated using the T45 method were significantly lower than those obtained using the adaptive threshold approach (Wilcoxon signed-ranks test, both P <0.001). Significant higher SUV_{max}, SUV mean and TLG were also evident (S3 Table), whereas all of the texture parameters showed no statistically significant differences. High ICCs were identified. SUV entropy and entropy revealed the lowest degrees of variation between PET/ACT and PET/HCT, whereas contrast and HGLZE continued to show large variations (S4 Table). Using the T45 method for validation purposes, the predictive role of SUV entropy and entropy from both PET/HCT and PET/ACT for DSS was confirmed using all of the three methodologies

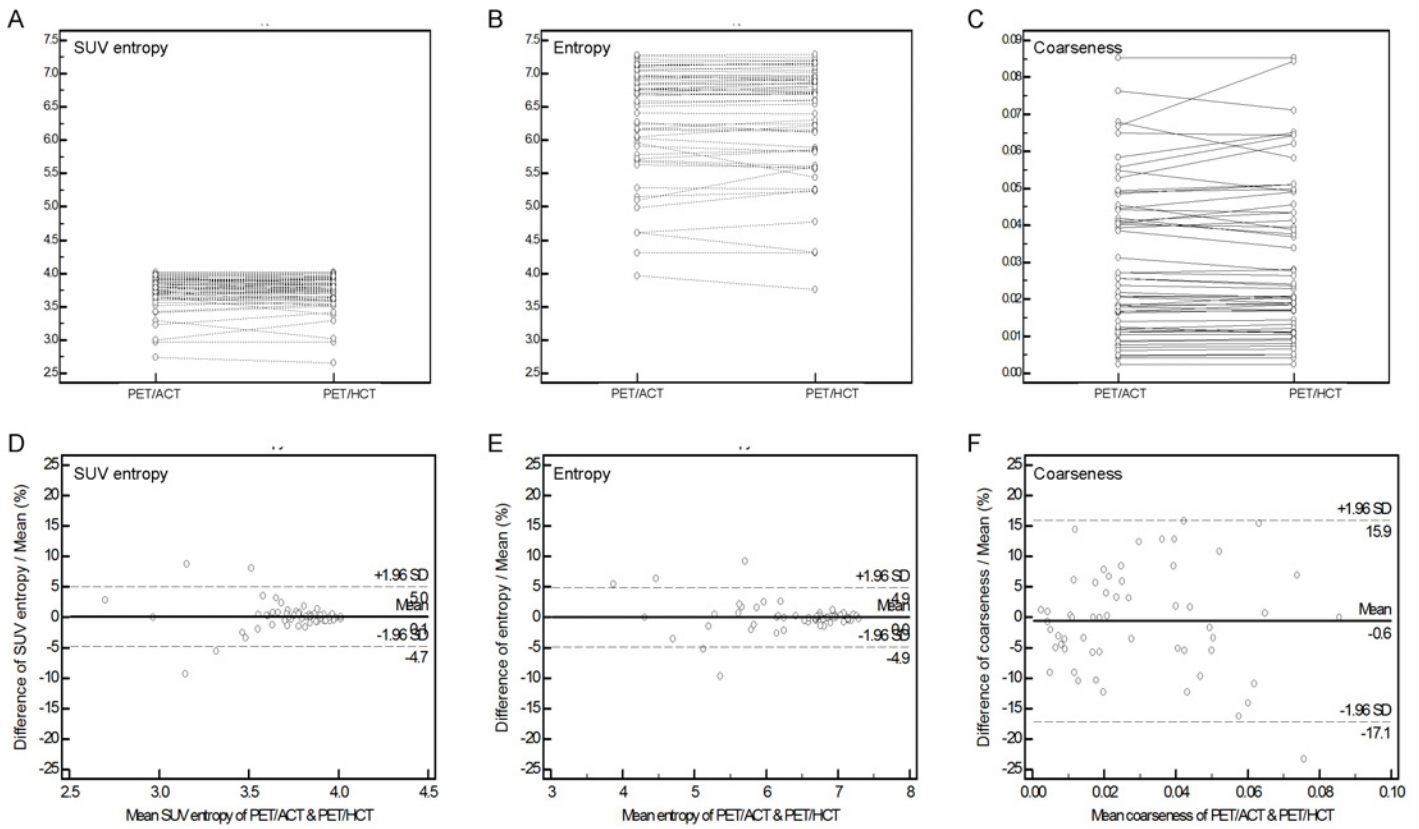

Fig 1. Dot-and-line diagrams of SUV entropy (A), entropy (B), and coarseness (C). Results of Bland-Altman analysis of SUV entropy (D), entropy (E), and coarseness (F).

doi:10.1371/journal.pone.0150509.g001

(ROC curves as well as univariate and multivariate Cox regression analyses). However, the role of coarseness remained significant only from PET/ACT (Table 5). Kaplan-Meier estimates of DSS for these analyses are reported in Fig 3.

Table 4. Univariate and multivariate Cox regression analyses of disease-specific survival using PET parameters.

Variables	Univariate analysis		Multivariate analysis[a]	
	HR (95% CI)	*P*	HR (95% CI)	*P*
PET/HCT				
SUV entropy	2.69 (1.37–5.29)	0.004	2.69 (1.32–5.45)	0.006
Entropy	2.81 (1.34–5.92)	0.006	2.69 (1.23–5.89)	0.013
Coarseness	0.38 (0.19–0.76)	0.007	0.34 (0.15–0.79)	0.012
PET/ACT				
SUV entropy	2.49 (1.24–4.99)	0.010	2.77 (1.32–5.83)	0.007
Entropy	2.81 (1.34–5.92)	0.006	2.69 (1.23–5.89)	0.013
Coarseness	0.38 (0.19–0.76)	0.007	0.34 (0.15–0.79)	0.012

HR: hazard ratio; CI: confidence interval.

[a]Adjusted for age, cell type, radical surgery, and AJCC stage (see text).

doi:10.1371/journal.pone.0150509.t004

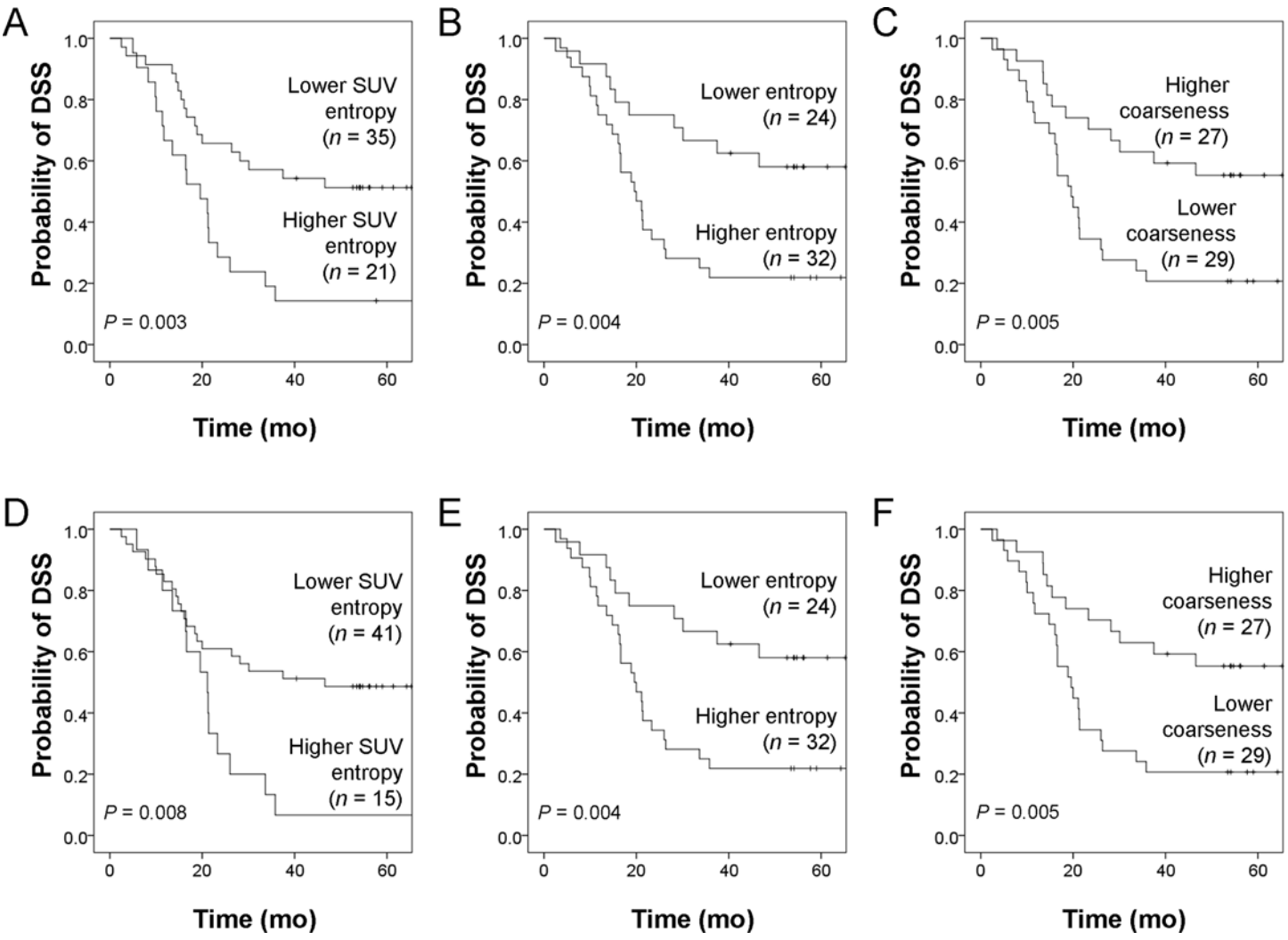

Fig 2. Kaplan-Meier estimates of disease-specific survival (DSS) from PET/HCT (A-C) and PET/ACT (D-F) parameters. Kaplan-Meier estimates of DSS stratified according to distinct cut-off values of PET/HCT and PET/ACT parameters. Cut-off values are shown in S2 Table. Log-rank test *P* values are also reported.

doi:10.1371/journal.pone.0150509.g002

Discussion

The quantification of PET images relies on accurate attenuation correction maps. However, respiration motion continues to remain a major challenge for PET/CT imaging. PET/HCT misregistration occurs when HCT imaging is performed during the inspiration [27–29, 51]. Accordingly, a displaced diaphragm by air-filled lung tissues results in an underestimation of the attenuation coefficient. Because PET/ACT can effectively reduce this issue, higher SUV_{max} values were identified in PET/ACT (especially for lesions located in the lower where a more marked respiratory motion was expected). In contrast, SUV_{max} values did not differ significant at sites different from the lower and background. Notably, texture indices obtained from PET/ACT and PET/HCT were largely similar even in the lower lung fields. Texture features are calculated using whole-tumor sampling and are useful for assessing the relationships between multiple voxels and their neighborhood (rather than a single voxel). Therefore, they are generally consistent even when different attenuation correction methods are used.

Table 5. Univariate and multivariate Cox regression analyses of disease-specific survival using PET parameters with tumor segmented with the T45 approach.

Variables	Univariate analysis		Multivariate [a]	
	HR (95% CI)	*P*	HR (95% CI)	*P*
PET/HCT				
SUV entropy	3.16 (1.58–6.35)	0.001	3.26 (1.52–6.99)	0.002
Entropy	4.52 (1.74–11.78)	0.002	3.87 (1.47–10.22)	0.006
Coarseness	0.46 (0.20–1.05)	0.066	0.42 (0.18–1.02)	0.056
PET/ACT				
SUV entropy	2.47 (1.20–5.09)	0.014	2.81 (1.29–6.09)	0.009
Entropy	3.74 (1.54–9.09)	0.004	3.13 (1.27–7.73)	0.013
Coarseness	0.28 (0.11–0.72)	0.008	0.26 (0.10–0.69)	0.007

HR: hazard ratio; CI: confidence interval.

[a]Adjusted for age, cell type, radical surgery and AJCC stage (see text).

doi:10.1371/journal.pone.0150509.t005

PET entropy has been shown to predict survival in patients with early-stage NSCLC [48]. In the current study, we were not only able to replicate this finding but we also showed that heterogeneous PET images were associated with unfavorable DSS. Heterogeneous images were characterized by larger values of SUV entropy and entropy. Notably, SUV entropy and entropy based on NGLCM from both PET/HCT and PET/ACT were significant predictors of survival. Moreover, SUV entropy and entropy remained consistent regardless of different PET reconstruction parameters (iteration number, FWHM, and pixel size) [49] and attenuation correction methods. NGTDM was originally developed to quantify human visual perception. A coarse image reflects the presence of a uniform intensity distribution, e.g. a homogeneous image. Although a previous study demonstrated a prognostic role of coarseness [8], this parameter shows a high extent of variation according to different segmentation methods, PET acquisition modes, and image reconstruction settings [45, 49, 52, 53]. As expected, coarseness values in this study were characterized by a marked extent of variation according to the attenuation correction method (33.0% and 55.0% for the adaptive threshold and T45 methods, respectively). Notably, coarseness was significantly associated with DSS using the adaptive threshold method. However, only a marginal association was observed when the T45 delineation without motion compensation was applied. In contrast, SUV entropy and entropy (which were characterized by a lower extent of variation) were significant in both PET/ACT and PET/HCT.

Different from our results, Yip et al. [54] reported significant differences between PET/HCT and 4D PET/CT for coarseness and busyness values. In 4D-PET/CT, 4D-CT images of five different respiratory phases are selected to match those of the corresponding 4D-PET acquired following PET/HCT. Consequently, the count of 4D-PET photons is different from that of PET/HCT, with a higher noise being evident for 4D PET (which may hamper the precise calculation of the texture features). The question as to whether such differences may have an impact on survival prediction remains open. Differently from 4D-PET/CT, PET/ACT uses the same PET images and all of the phases of PET signals are utilized. This observation may explain the limited differences in terms of texture parameters between PET/HCT and PET/ACT.

Our findings emphasize the importance of using a standardized approach for PET texture analysis [55] in NSCLC patients. It may be argued that the diversity of PET texture parameters (resulting from differences in target segmentation, rebin process, reconstruction settings, and/or terminology) may hamper the application of texture-based analysis in clinical practice [53].

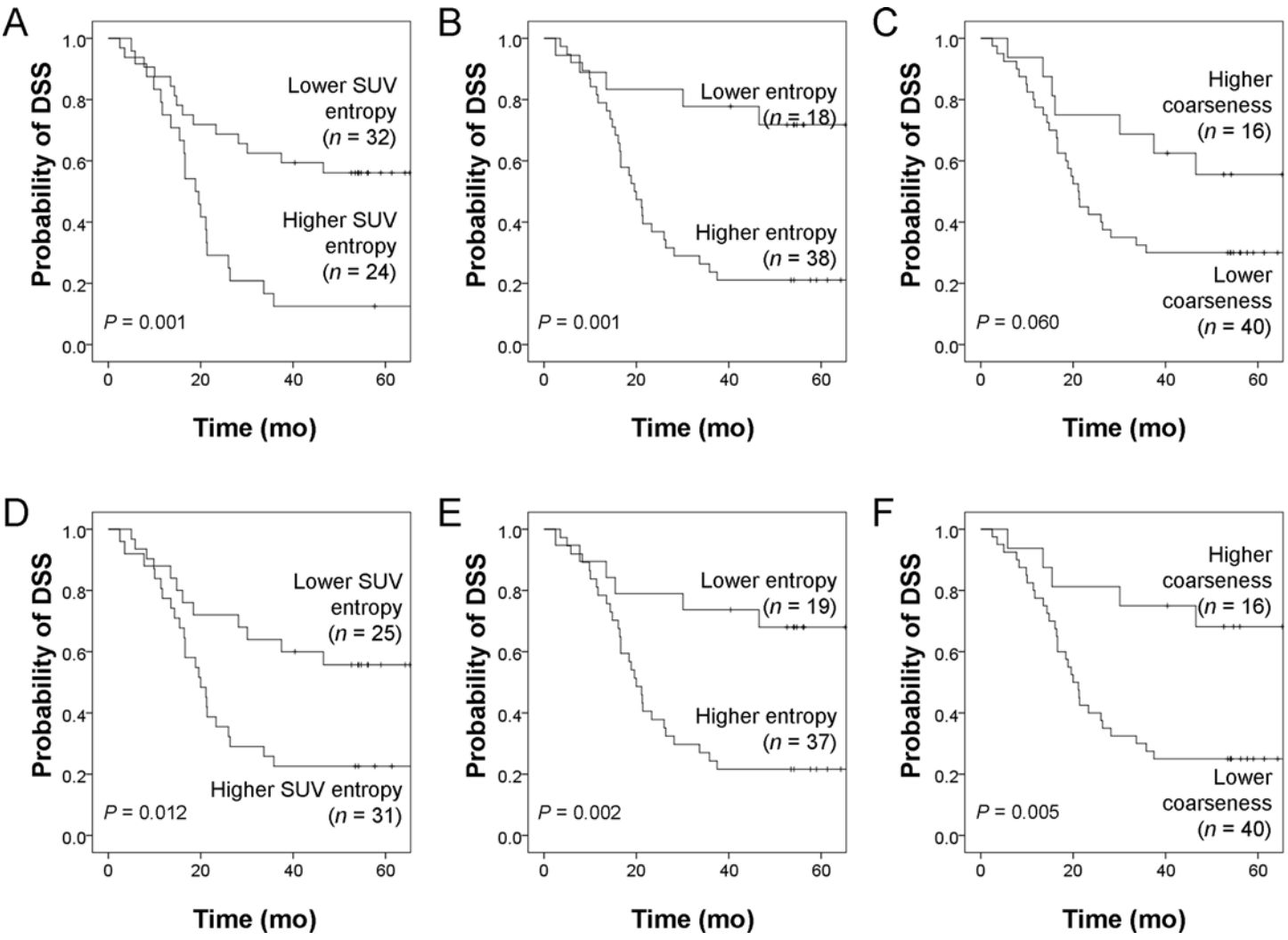

Fig 3. Kaplan-Meier estimates of disease-specific survival (DSS) for PET/HCT (A-C) and PET/ACT (D-F) parameters segmented by T45. Kaplan-Meier estimates of DSS rates stratified according to distinct cut-off values of PET/HCT and PET/ACT parameters. Cut-off values are shown in S2 Table. Log-rank test *P* values are also reported.

doi:10.1371/journal.pone.0150509.g003

However, technical advances and the implementation of randomized clinical trials will hopefully be helpful in overcoming such challenges [2, 56]. It is also possible that texture parameters (especially SUV entropy and entropy) can be useful in guiding radiotherapy. In this regard, it would be clinically relevant to assess the value of dose painting using unfixed radiation dose distribution to the tumor (based on image-guided stratification of high-risk target volumes). Although dose painting based on PET images with high SUV does not seem to be clinically useful for predicting outcomes [57], the identification of high-risk subvolumes based on PET texture parameters or multiparametric imaging [58] may warrant further investigation.

Several limitations of our study merit comment. Because of the retrospective nature of the study, a selection bias cannot be excluded. Our results related to the predictive value of SUV entropy and entropy need to be independently validated in longitudinal studies. Another caveat inherent in our study is the use of two methods (i.e., adaptive threshold and T45) for tumor delineation. Further studies are necessary to clarify the potential impact of the tumor delineation method on the prognostic significance of the indexes. Finally, we did not

specifically investigate the impact of the reconstruction algorithms on the texture features [45] and their effect on survival.

Conclusions

The results of our study indicate that texture features obtained with PET/HCT and PET/ACT showed limited differences and good levels of agreement regardless of the delineation method used. We also showed that texture parameters from PET/ACT are clinically useful in the prediction of survival in NSCLC patients and that SUV entropy and entropy are robust attenuation correction methods.

Supporting Information

S1 Fig. Results of Bland-Altman analysis. SUVmax (A), SUV mean (B), TLG (C), uniformity (D), dissimilarity (E), homogeneity (F), busyness (G), contrast (H), complexity (I), grey-level nonuniformity (J), zone-size nonuniformity (K), and high grey-level large zone emphasis (L).
(TIF)

S1 Table. Results of Wilcoxon signed-ranks test for different PET parameters according to tumor location in the lung.
(DOCX)

S2 Table. Optimal cut-off values for different PET parameters in the prediction of 3-year disease-specific survival.
(DOCX)

S3 Table. Results of Wilcoxon signed-ranks tests for PET/HCT and PET/ACT parameters using T45 segmentation.
(DOCX)

S4 Table. Intraclass correlation coefficients and Bland-Altman analyses for PET parameters using T45 segmentation.
(DOCX)

S5 Table. Complete list of univariate and multivariate Cox regression analyses for the prediction of disease-specific survival using texture parameters.
(DOCX)

Acknowledgments

Averaged CT for attenuation correction of PET was originally developed by Dr. Tinsu Pan (University of Texas, M.D. Anderson Cancer Center). We are grateful to Dr. Pan for the generous sharing of his software.

Author Contributions

Conceived and designed the experiments: NMC CHH TCY. Performed the experiments: NMC YHDF DLT. Analyzed the data: NMC CHH TCY. Contributed reagents/materials/analysis tools: NMC YHDF DLT CHH TCY. Wrote the paper: NMC CHH TCY.

References

1. Lee CK, Brown C, Gralla RJ, Hirsh V, Thongprasert S, Tsai CM, et al. Impact of EGFR inhibitor in non-small cell lung cancer on progression-free and overall survival: a meta-analysis. J Natl Cancer Inst. 2013; 105(9):595–605. doi: 10.1093/jnci/djt072 PMID: 23594426

2. Lambin P, Roelofs E, Reymen B, Velazquez ER, Buijsen J, Zegers CM, et al. 'Rapid Learning health care in oncology'—an approach towards decision support systems enabling customised radiotherapy'. Radiat Oncol. 2013; 109(1):159–64.
3. Borst GR, Belderbos JS, Boellaard R, Comans EF, De Jaeger K, Lammertsma AA, et al. Standardised FDG uptake: a prognostic factor for inoperable non-small cell lung cancer. Eur J Cancer. 2005; 41 (11):1533–41. PMID: 15953716
4. Lee KH, Lee SH, Kim DW, Kang WJ, Chung JK, Im SA, et al. High fluorodeoxyglucose uptake on positron emission tomography in patients with advanced non-small cell lung cancer on platinum-based combination chemotherapy. Clin Cancer Res 2006; 12(14):4232–6. PMID: 16857796
5. Chen HH, Chiu NT, Su WC, Guo HR, Lee BF. Prognostic value of whole-body total lesion glycolysis at pretreatment FDG PET/CT in non-small cell lung cancer. Radiology. 2012; 264(2):559–66. doi: 10.1148/radiol.12111148 PMID: 22692034
6. Liao S, Penney BC, Wroblewski K, Zhang H, Simon CA, Kampalath R, et al. Prognostic value of metabolic tumor burden on 18F-FDG PET in nonsurgical patients with non-small cell lung cancer. Eur J Nucl Med Mol Imaging 2012; 39(1):27–38. doi: 10.1007/s00259-011-1934-6 PMID: 21946983
7. Gerlinger M, Rowan AJ, Horswell S, Larkin J, Endesfelder D, Gronroos E, et al. Intratumor heterogeneity and branched evolution revealed by multiregion sequencing. N Engl J Med. 2012; 366(10):883–92. doi: 10.1056/NEJMoa1113205 PMID: 22397650
8. Cook GJ, Yip C, Siddique M, Goh V, Chicklore S, Roy A, et al. Are pretreatment 18F-FDG PET tumor textural features in non-small cell lung cancer associated with response and survival after chemoradiotherapy? J Nucl Med. 2013; 54(1):19–26. doi: 10.2967/jnumed.112.107375 PMID: 23204495
9. Vaidya M, Creach KM, Frye J, Dehdashti F, Bradley JD, El Naqa I. Combined PET/CT image characteristics for radiotherapy tumor response in lung cancer. Radiother Oncol. 2012; 102(2):239–45. doi: 10.1016/j.radonc.2011.10.014 PMID: 22098794
10. El Naqa I. The role of quantitative PET in predicting cancer treatment outcomes. Clinical and Translational Imaging. 2014; 2(4):305–20.
11. Hatt M, Majdoub M, Vallières M, Tixier F, Le Rest CC, Groheux D, et al. 18F-FDG PET uptake characterization through texture analysis: investigating the complementary nature of heterogeneity and functional tumor volume in a multi-cancer site patient cohort. J Nucl Med. 2015; 56(1):38–44. doi: 10.2967/jnumed.114.144055 PMID: 25500829
12. El Naqa I, Grigsby P, Apte A, Kidd E, Donnelly E, Khullar D, et al. Exploring feature-based approaches in PET images for predicting cancer treatment outcomes. Pattern Recognit. 2009; 42(6):1162–71. PMID: 20161266
13. Tixier F, Le Rest CC, Hatt M, Albarghach N, Pradier O, Metges JP, et al. Intratumor heterogeneity characterized by textural features on baseline 18F-FDG PET images predicts response to concomitant radiochemotherapy in esophageal cancer. J Nucl Med 2011; 52(3):369–78. doi: 10.2967/jnumed.110.082404 PMID: 21321270
14. Cheng NM, Fang DY, Chang JT, Huang CG, Tsan DL, Ng SH, et al. Texture features of pretreatment 18F FDG PET/CT images: prognostic significance in patients with advanced T-stage oropharyngeal squamous cell carcinoma. J Nucl Med. 2013; 54(10):1703–9. doi: 10.2967/jnumed.112.119289 PMID: 24042030
15. Chicklore S, Goh V, Siddique M, Roy A, Marsden PK, Cook GJ. Quantifying tumour heterogeneity in (18)F-FDG PET/CT imaging by texture analysis. Eur J Nucl Med Mol Imaging. 2013; 40(1):133–40. doi: 10.1007/s00259-012-2247-0 PMID: 23064544
16. Tan S, Kligerman S, Chen W, Lu M, Kim G, Feigenberg S, et al. Spatial-temporal [¹ F]FDG-PET features for predicting pathologic response of esophageal cancer to neoadjuvant chemoradiation therapy. Int J Radiat Oncol Biol Phys. 2013; 85(5):1375–82. doi: 10.1016/j.ijrobp.2012.10.017 PMID: 23219566
17. Yang F, Thomas MA, Dehdashti F, Grigsby PW. Temporal analysis of intratumoral metabolic heterogeneity characterized by textural features in cervical cancer. Eur J Nucl Med Mol Imaging 2013; 40 (5):716–27. doi: 10.1007/s00259-012-2332-4 PMID: 23340594
18. Tixier F, Groves AM, Goh V, Hatt M, Ingrand P, Le Rest CC, et al. Correlation of intra-tumor 18F-FDG uptake heterogeneity indices with perfusion CT derived parameters in colorectal cancer. PLoS One. 2014; 9(6):e99567. doi: 10.1371/journal.pone.0099567 eCollection 2014 PMID: 24926986
19. Cheng NM, Fang YH, Lee LY, Chang JT, Tsan DL, Ng SH, et al. Zone-size nonuniformity of 18F-FDG PET regional textural features predicts survival in patients with oropharyngeal cancer. Eur J Nucl Med Mol Imaging. 2015; 42(3):419–28. doi: 10.1007/s00259-014-2933-1 PMID: 25339524
20. Wang HM, Cheng NM, Lee LY, Fang YD, Chang JT, Tsan DL, et al. Heterogeneity of 18 F-FDG PET combined with expression of EGFR may improve the prognostic stratification of advanced oropharyngeal carcinoma. Int J Cancer. 2015;Aug 27. doi: 10.1002/ijc.29811 [Epub ahead of print].

21. Lambin P, Rios-Velazquez E, Leijenaar R, Carvalho S, van Stiphout RG, Granton P, et al. Radiomics: extracting more information from medical images using advanced feature analysis. Eur J Cancer. 2012; 48(4):441–6. doi: 10.1016/j.ejca.2011.11.036 PMID: 22257792

22. Aerts HJ, Velazquez ER, Leijenaar RT, Parmar C, Grossmann P, Carvalho S, et al. Decoding tumour phenotype by noninvasive imaging using a quantitative radiomics approach. Nat Commun 2014;Jun 3; 5:4006. doi: 10.1038/ncomms5006 PMID: 24892406

23. Cook GJ, Siddique M, Taylor BP, Yip C, Chicklore S, Goh V. Radiomics in PET: principles and applications. Clinical and Translational Imaging. 2014; 2(3):269–76.

24. Parmar C, Rios Velazquez E, Leijenaar R, Jermoumi M, Carvalho S, Mak RH, et al. Robust radiomics feature quantification using semiautomatic volumetric segmentation. PLoS One. 2014; 9(7):e102107. doi: 10.1371/journal.pone.0102107 eCollection 2014 PMID: 25025374

25. Coroller TP, Grossmann P, Hou Y, Rios Velazquez E, Leijenaar RT, Hermann G, et al. CT-based radiomic signature predicts distant metastasis in lung adenocarcinoma. Radiother Oncol. 2015; 114(3):345–50. doi: 10.1016/j.radonc.2015.02.015 PMID: 25746350

26. Parmar C, Leijenaar RT, Grossmann P, Rios Velazquez E, Bussink J, Rietveld D, et al. Radiomic feature clusters and prognostic signatures specific for Lung and Head & Neck cancer. Sci Rep. 2015;Jun 5; 5:11044. doi: 10.1038/srep11044 PMID: 26251068

27. Cohade C, Osman M, Marshall LN, Wahl RN. PET-CT: accuracy of PET and CT spatial registration of lung lesions. Eur J Nucl Med Mol Imaging. 2003; 30(5):721–6. PMID: 12612809

28. Goerres GW, Burger C, Kamel E, Seifert B, Kaim AH, Buck A, et al. Respiration-induced attenuation artifact at PET/CT: technical considerations. Radiology. 2003; 226(3):906–10. PMID: 12616024

29. Osman MM, Cohade C, Nakamoto Y, Marshall LT, Leal JP, Wahl RL. Clinically significant inaccurate localization of lesions with PET/CT: frequency in 300 patients. J Nucl Med 2003; 44(2):240–3. PMID: 12571215

30. Erdi YE, Nehmeh SA, Pan T, Pevsner A, Rosenzweig KE, Mageras G, et al. The CT motion quantitation of lung lesions and its impact on PET-measured SUVs. J Nucl Med. 2004; 45(8):1287–92. PMID: 15299050

31. Pan T, Mawlawi O, Nehmeh SA, Erdi YE, Luo D, Liu HH, et al. Attenuation correction of PET images with respiration-averaged CT images in PET/CT. J Nucl Med. 2005; 46(9):1481–7. PMID: 16157531

32. Pan T, Lee TY, Rietzel E, Chen GT. 4D-CT imaging of a volume influenced by respiratory motion on multi-slice CT. Med Phys. 2004; 31(2):333–40. PMID: 15000619

33. Cheng NM, Yu CT, Ho KC, Wu YC, Liu YC, Wang CW, et al. Respiration-averaged CT for attenuation correction in non-small-cell lung cancer. Eur J Nucl Med Mol Imaging. 2009; 36(4):607–15. doi: 10.1007/s00259-008-0995-7 PMID: 19050875

34. Kuo WH, Kuo WH, Wu YC, Wu CY, Ho KC, Chiu PH, et al. Node/aorta and node/liver SUV ratios from (18)F-FDG PET/CT may improve the detection of occult mediastinal lymph node metastases in patients with non-small cell lung carcinoma. Acad Radiol. 2012; 19(6):685–92. doi: 10.1016/j.acra.2012.02.013 PMID: 22459646

35. Nehmeh SA, Erdi YE, Pan T, Yorke E, Mageras GS, Rosenzweig KE, et al. Quantitation of respiratory motion during 4D-PET/CT acquisition. Med Phys. 2004; 31(6):1333–8. PMID: 15259636

36. Alessio AM, Kohlmyer S, Branch K, Chen G, Caldwell J, Kinahan P. Cine CT for attenuation correction in cardiac PET/CT. J Nucl Med. 2007; 48(5):794–801. PMID: 17475969

37. Chi PC, Mawlawi O, Nehmeh SA, Erdi YE, Balter PA, Luo D, et al. Design of respiration averaged CT for attenuation correction of the PET data from PET/CT. Med Phys. 2007; 34(6):2039–47. PMID: 17654907

38. Pan T, Mawlawi O, Luo D, Liu HH, Chi PC, Mar MV, et al. Attenuation correction of PET cardiac data with low-dose average CT in PET/CT. Med Phys. 2006; 33(10):3931–8. PMID: 17089855

39. Nestle U, Kremp S, Schaefer-Schuler A, Sebastian-Welsch C, Hellwig D, Rübe C, et al. Comparison of different methods for delineation of 18F-FDG PET-positive tissue for target volume definition in radiotherapy of patients with non-Small cell lung cancer. J Nucl Med. 2005; 46(8):1342–8. PMID: 16085592

40. Larson SM, Erdi Y, Akhurst T, Mazumdar M, Macapinlac HA, Finn RD, et al. Tumor treatment response based on visual and quantitative changes in global tumor glycolysis using PET-FDG imaging. The visual response score and the change in total lesion glycolysis. Clin Positron Imaging. 1999; 2(3):159–71. PMID: 14516540

41. Haralick Robert M., Shanmugam K., Dinstein I. Textural features for image classification. IEEE Trans Syst Man Cybern. 1973; 3(6):610–21.

42. Clausi DA. An analysis of co-occurrence texture statistics as a function of grey level quantization. Can J Remote Sensing. 2002; 28(1):45–62.

43. Amadasun M., King R. Textural features corresponding to textural properties. IEEE Trans Syst Man Cybern. 1989; 19(5):1264–74.

44. Tang X. Texture information in run-length matrices. IEEE Trans Image Process 1998; 7(11):1602–9. doi: 10.1109/83.725367 PMID: 18276225

45. Galavis PE, Hollensen C, Jallow N, Paliwal B, Jeraj R. Variability of textural features in FDG PET images due to different acquisition modes and reconstruction parameters. Acta Oncol. 2010; 49 (7):1012–6. doi: 10.3109/0284186X.2010.498437 PMID: 20831489

46. Leijenaar RT, Carvalho S, Velazquez ER, van Elmpt WJ, Parmar C, Hoekstra OS, et al. Stability of FDGPET Radiomics features: An integrated analysis of test-retest and inter-observer variability. Acta Oncol. 2013; 52(7):1391–7. doi: 10.3109/0284186X.2013.812798 PMID: 24047337

47. Hatt M, Tixier F, Cheze Le Rest C, Pradier O, Visvikis D. Robustness of intratumour 18F-FDG PET uptake heterogeneity quantification for therapy response prediction in oesophageal carcinoma. Eur J Nucl Med Mol Imaging. 2013; 40(11):1662–7. doi: 10.1007/s00259-013-2486-8 PMID: 23857457

48. Pyka T, Bundschuh RA, Andratschke N, Mayer B, Specht HM, Papp L, et al. Textural features in pre-treatment [F18]-FDG-PET/CT are correlated with risk of local recurrence and disease-specific survival in early stage NSCLC patients receiving primary stereotactic radiation therapy. Radiat Oncol. 2015;Apr 22; 10:100. doi: 10.1186/s13014-015-0407-7 PMID: 25900186

49. Yan J, Chu-Shern JL, Loi HY, Khor LK, Sinha AK, Quek ST, et al. Impact of Image Reconstruction Settings on Texture Features in 18F-FDG PET. J Nucl Med. 2015; 56(11):1667–73. doi: 10.2967/jnumed.115.156927 PMID: 26229145

50. Fang YH, Lin CY, Shih MJ, Wang HM, Ho TY, Liao CT, et al. Development and evaluation of an open-source software package "CGITA" for quantifying tumor heterogeneity with molecular images. Biomed Res Int. 2014; 2014:248505. doi: 10.1155/2014/248505 PMID: 24757667

51. Goerres GW, Kamel E, Heidelberg TN, Schwitter MR, Burger C, von Schulthess GK. PET-CT image coregistration in the thorax: influence of respiration. Eur J Nucl Med Mol Imaging 2002; 29(3):351–60. PMID: 12002710

52. Orlhac F, Soussan M, Maisonobe JA, Garcia CA, Vanderlinden B, Buvat I. Tumor texture analysis in 18F-FDG PET: relationships between texture parameters, histogram indices, standardized uptake values, metabolic volumes, and total lesion glycolysis. J Nucl Med. 2014; 55(3):414–22. doi: 10.2967/jnumed.113.129858 PMID: 24549286

53. Buvat I, Orlhac F, Soussan M. Tumor Texture Analysis in PET: Where Do We Stand? J Nucl Med. 2015; 56(11):1642–4. doi: 10.2967/jnumed.115.163469 PMID: 26294296

54. Yip S, McCall K, Aristophanous M, Chen AB, Aerts HJ, Berbeco R. Comparison of Texture Features Derived from Static and Respiratory-Gated PET Images in Non-Small Cell Lung Cancer. PLoS One. 2014; 9(12):e115510. doi: 10.1371/journal.pone.0115510 PMID: 25517987

55. Leijenaar RT, Nalbantov G, Carvalho S, van Elmpt WJ, Troost EG, Boellaard R, et al. The effect of SUV discretization in quantitative FDG-PET Radiomics: the need for standardized methodology in tumor texture analysis. Sci Rep. 2015;Aug 5; 5:11075. doi: 10.1038/srep11075 PMID: 26242464

56. Lambin P, Zindler J, Vanneste B, van de Voorde L, Jacobs M, Eekers D, et al. Modern clinical research: How rapid learning health care and cohort multiple randomised clinical trials complement traditional evidence based medicine. Acta Oncol. 2015; 54(9):1289–300. doi: 10.3109/0284186X.2015.1062136 PMID: 26395528

57. Trani D, Yaromina A, Dubois L, Granzier M, Peeters SG, Biemans R, et al. Preclinical Assessment of Efficacy of Radiation Dose Painting Based on Intratumoral FDG-PET Uptake. Clin Cancer Res. 2015; 21(24):5511–8. doi: 10.1158/1078-0432.CCR-15-0290 PMID: 26276892

58. van Elmpt W, Zegers CM, Reymen B, Even AJ, Dingemans AC, Oellers M, et al. Multiparametric imaging of patient and tumour heterogeneity in non-small-cell lung cancer: quantification of tumour hypoxia, metabolism and perfusion. Eur J Nucl Med Mol Imaging. 2015;Sep 4. [Epub ahead of print].